RESEARCH ARTICLE

Lanthanide-MOFs as multifunctional luminescent sensors†

Sibo Wang,[a] Bo Sun,[b] Zhongmin Su, [iD] *[b] Guohui Hong,[a] Xiao Li,*[c,b] Yanling Liu,[d] Qingqing Pan[b] and Jing Sun*[b]

Five isostructural lanthanide metal–organic frameworks [Ln(BDPO)(H$_2$O)$_4$] (Ln = Eu for CUST-623, Tb for CUST-624, Gd for CUST-625, Dy for CUST-626, and Sm for CUST-627, BDPO = N,N' bis(3,5-dicarboxy-phenyl)-oxalamide) were synthesized by the solvothermal method. Single-crystal X-ray diffraction shows that Ln-MOFs manifest framework structures with two kinds of 1D open channels in the *b*-axis direction. Dual emission luminescent thermometer films were successfully prepared by immobilizing Eu$_x$Tb$_{0.02-x}$-BDPO into polyvinyl alcohol (PVA) aqueous solution, which features the integrity of MOF powders, proving their excellent processability. Moreover, Eu$_{0.002}$Tb$_{0.018}$-BDPO@PVA shows excellent temperature sensing performance with a high sensitivity of 3.7% K^{-1} in the temperature range of 303 K–423 K. CUST-623 and CUST-624 can be used as multiresponse fluorescent sensors for detecting Fe^{3+}, Cr$_2$O$_7^{2-}$, CrO$_4^{2-}$ and TNP. In addition, the mechanism of fluorescence sensing is investigated by infrared (IR) spectroscopy, powder X-ray diffraction (PXRD) and ultraviolet–visible (UV-vis) spectroscopy. This work provides a general method for constructing Ln-MOF sensor materials with multifunctional luminescence characteristics.

1. Introduction

The living environment of humankind is facing diverse challenges due to industrial development and increasing population.[1] Excessive emission of pollutants, which can quickly spread to air, soil and water, has become a pressing global problem, triggering a serious threat to the environment and biological health.[2] In industrial waste, heavy metal contaminations, due to the extreme toxicity and non-biodegradability, lead to a variety of incurable diseases and seriously affect biological health.[3] Meanwhile, nitroaromatics are also considered to be serious pollutants in the environment, which endanger

human health and disrupt social security.[4] Thereinto, the excessive usage of TNP molecules, which are the most essential raw materials for explosives, affects the decomposition of organisms in the aquatic environment and can cause serious health dilemmas.[5] At present, conventional inspection methods rely mainly on detection instruments, which require frequent and careful calibration and maintenance, with many inconveniences.[6] More and more researchers are focusing on the fluorescence sensing method, which exhibits high sensitivity, high selectivity and simple operation. Hence, it is necessary and urgent to develop affordable, convenient, fast and sensitive detection tools for real-time analyte detection.[7]

Temperature is a fundamental physical quantity whose precise measurement has great significance in science and industry.[8] Traditional thermometers are primarily based on contact measurements, restricted in many practical situations.[9] Luminescence temperature measurements have been authenticated to be a promising temperature measurement method owing to the advantages of being non-invasive, convenient, and sensitive in the temperature measurement process.[10] Luminescent thermometer measurements mainly depend on the change of luminescence intensity or fluorescence lifetime with temperature changes.[11] Luminescent thermometers are mainly divided into two types: single and double luminescent centers, among which dual luminescent centers can be constructed into ratiometric luminescent thermometers, possessing higher accuracy in the temperature

[a]School of Materials Science and Engineering, Changchun University of Science and Technology, Changchun 130022, People's Republic of China

[b]School of Chemistry and Environmental Engineering, Changchun University of Science and Technology, Jilin Provincial Science and Technology Innovation Center of Optical Materials and Chemistry, Jilin Provincial International Joint Research Center of Photofunctional Materials and Chemistry, Changchun, 130022, People's Republic of China

[c]Laboratory of Preparation and Application of Environmental Friendly Materials (Jilin Normal University), Ministry of Education, Changchun, 130103, People's Republic of China

[d]Chemistry and Chemical Engineering, Hainan Normal University, Hainan, 571158, People's Republic of China

This journal is © the Partner Organisations 2022

Inorg. Chem. Front., 2022, **9**, 3259–3266 | **3259**

measurement process.[12] Such luminescent thermometers can be applied to fast-moving objects, biological systems, strong electromagnetic fields, *etc*. At present, luminescent materials for temperature measurements include organic dyes, fluorescent probes, phosphors, quantum dots, and organic–inorganic hybrid materials (complexes and MOFs).[13]

As emerging porous materials, luminescent metal–organic frameworks (LMOFs) have received extensive attention due to their rich structures, high surface areas, adjustable pores, *etc*.[14] In LMOFs, fluorescence is produced mainly from organic ligands, luminescent guests or metal ions. Due to the special luminescence characteristics of lanthanide metal ions, lanthanide metal–organic frameworks (Ln-MOFs) have been comprehensively used in tunable phosphors, fluorescent sensors, and luminescent temperature sensors.[15] Different Ln^{3+} ions doped in isomorphic Ln-MOFs to fabricate luminescent thermometers possess the advantages of high precision, self-calibration, and high resolution, and have become a greatly promising tool for ratiometric temperature measurements.[16] Thereinto, the detection of harmful substances, such as heavy metals, explosives, small organic molecules, antibiotics, *etc*., by fluorescence sensing technology has received widespread attention.[17] In Ln-MOFs, organic ligands as sensitizers can effectively transfer energy to lanthanide metals, making Ln-MOFs possess high luminescence intensity. Among the multifunctional ligands, organic moieties with a π-conjugated system can effectively sensitize Ln^{3+} ions through the antenna effect, resulting in enhanced overall luminous intensity.[18]

For practical applications, incorporation of metal–organic framework powders into organic polymers is a straightforward and effective strategy for the development of novel composites that combine the excellent properties of MOFs with the robustness of organic polymers.[19] Meanwhile, polymers are the ideal base for providing unique softness, thermal and chemical stability, and photoelectric properties.[20] The functionality of Ln-MOFs is combined with the flexibility and machinability of polymers by physical mixing methods to prepare functional composite films used in luminescence fields.[21] Membranes with optical functions can be directly produced in factories and applied in practical situations, largely expanding the scope of application and improving the utilization efficiency.[22] In summary, the use of Ln-MOFs and polymer composites as luminescent materials deserves attention.

In this work, five isomorphic Ln-MOFs were successfully synthesized using H_6BDPO and lanthanide metal ions. Employing polyvinyl alcohol (PVA) as the polymer substrate, $Eu_xTb_{0.02-x}$-BDPO@PVA polymer membranes were synthesized by physical mixing. These membranes retain the crystallinity and luminescence properties of $Eu_xTb_{0.02-x}$-BDPO as well as the flexibility of polymers. Subsequently, we systematically researched the temperature sensing performance of $Eu_xTb_{0.02-x}$-BDPO and $Eu_xTb_{0.02-x}$-BDPO@PVA. In the temperature range of 303 K–423 K, $Eu_xTb_{0.02-x}$-BDPO@PVA was used as a ratiometric luminescent thermometer, which can realize visible color changes, which can be observed with the naked eye with a high sensitivity of 3.7% K^{-1}. Furthermore,

CUST-623 and CUST-624 exhibit fluorescence quenching effects on Fe^{3+}, $Cr_2O_7^{2-}$, CrO_4^{2-}, and TNP, and the detection limits are in the low-level range, achieving the ppm level for the detection of TNP.

2. Experimental section

2.1 Synthesis of Ln-MOFs

A mixture of $Ln(NO_3)_3 \cdot 6H_2O$ (20 mg, 0.06 mmol) (Ln = Eu, Tb, Gd, Dy, Sm) and H_6BDPO (10 mg, 0.03 mmol) is dissolved in DMA (3 mL), deionized water (3 mL) and six drops of formic acid, and then the mixture is put into a sealed 10 mL vial and heated at 80 °C for 72 h and cooled to room temperature in 12 hours. Colorless block crystals were obtained and washed with DMA and H_2O. The synthesis of $Eu_xTb_{0.02-x}$-BDPO, film preparation and other experimental details are shown in the ESI.†

3. Results and discussion

3.1 Structure description of Ln-MOFs

CUST-623–CUST-627 possess the same crystal structure, so CUST-623 is selected as the representative for discussion. Single crystal data analysis shows that CUST-623 crystallizes in the monoclinic system with the $P2_1/c$ space group. The asymmetric unit contains one Eu^{3+}, a fully deprotonated $BDPO^{6-}$ ligand, and four coordinated H_2O molecules. Each Eu atom possesses a nine-coordination mode, in which five oxygen atoms come from the carboxyl groups of three $BDPO^{6-}$ ligands, and four oxygen atoms come from coordinated water molecules (Fig. 1a). The asymmetric units build framework structures through $BDPO^{6-}$ linkers. Fig. 1b shows dual alternating channels from the *b*-axis direction. In topological ana-
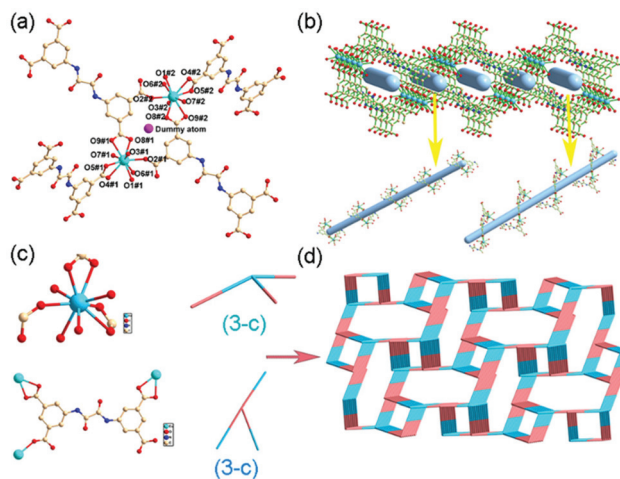

Fig. 1 (a) Coordination environment of Eu^{3+}. (b) 3D framework in the *b*-axis of CUST-623. (c) Node splitting diagram. (d) The topological structure of CUST-623.

3260 | *Inorg. Chem. Front.*, 2022, **9**, 3259–3266

This journal is © the Partner Organisations 2022

lysis, the ligand and the metal center are 3-linked points (Fig. 1c). The dot symbol is $\{4\cdot8^2\}$ in TOPOS software (Fig. 1d).

3.2 Stability of Ln-MOFs

The thermal stability of Ln-MOFs was studied under a N_2 atmosphere from 25 to 800 °C (Fig. S1†). Ln-MOFs exhibit similar TGA curves, so we selected CUST-623 as a representative example to analyze their thermal stability. From 25 to 158 °C, the weight lost is 11.95% (calculated, 11.32%) due to the loss of coordinated water molecules. Subsequently, the framework collapsed. The PXRD patterns of Ln-MOFs are shown in Fig. S2.† The peaks in the PXRD patterns are consistent with single-crystal X-ray simulation results, proving the good phase purity. Furthermore, the stability performance in water was studied on CUST-623 and CUST-624, and the PXRD results show that the PXRD peak position remains unchanged after as long as seven days of immersion in water, which proves satisfactory water stability (Fig. S3†). As expected, the PXRD peak positions of $Eu_xTb_{0.02-x}$-BDPO are consistent with those of Ln-MOFs (Fig. S4†). Inductively coupled plasma (ICP) spectroscopy confirms the metal content of $Eu_xTb_{0.02-x}$-BDPO (Table S4†).

3.3 Luminescence properties

The antenna effect is commonly presented in Ln-MOFs, where organic ligands acting as "antennas" are effectively sensitized to Ln^{3+} ions, ensuring stronger emissions as a whole.[23] According to the literature the single re-excited state energy of the ligand $\Delta E = 3.77 \times 10^4$ cm^{-1} (4.69 eV). The triple excitation energy $\Delta E1$ is 1.84×10^4 (2.29 eV).[24] Referring to Reinhold's rule of thumb,[25] the energy difference between ΔE and $\Delta E1$ is $\Delta E2 = 1.94 \times 10^4$ cm^{-1} (2.40 eV), much higher than that of the ISC (5000 cm^{-1}) process (Scheme S1†). Therefore, the energy in the ligand is easily transferred to Ln^{3+}. The solid-state excitation spectra and the emission spectra of H_6BDPO and Ln-MOFs were studied at room temperature (Fig. S5 and S6†). H_6BDPO shows luminescence at $\lambda_{em} = 425$ nm ($\lambda_{ex} = 352$) due to π–π charge transfer. The fluorescence spectra of Ln-MOFs present the characteristic emission peaks of lanthanide ions and the H_6BDPO ligand. The emission peaks of CUST-623 at 580 nm, 593 nm, 617 nm, 651 nm, and 700 nm are attributed to $^5D_0$–^7F_J ($J = 0$–4), in which $^5D_0$–$^7F_2$ (617 nm) occupies the entire spectrum, exhibiting red light (Fig. 2a). The emission spectrum of CUST-624 consists of four emission peaks at 494 nm, 547 nm, 587 nm, and 622 nm, attributed to $^5D_4$–^7F_J ($J = 6, 5, 4, 3$), where $^5D_4$–$^7F_5$ (547 nm) is the most prominent one, resulting in green light emission (Fig. 2b). CUST-625–CUST-627 are dominated by the wide emission belt emitted by ligands (Fig. S6†). $Eu_xTb_{0.02-x}$-BDPO possesses the characteristic emission of Eu and Tb (Fig. 2c). As the Eu content increases, the color changes from green to red under a UV lamp (Fig. 2d). Based on the above results, the emission color can be easily changed by adjusting the content ratio of Eu and Tb ions.
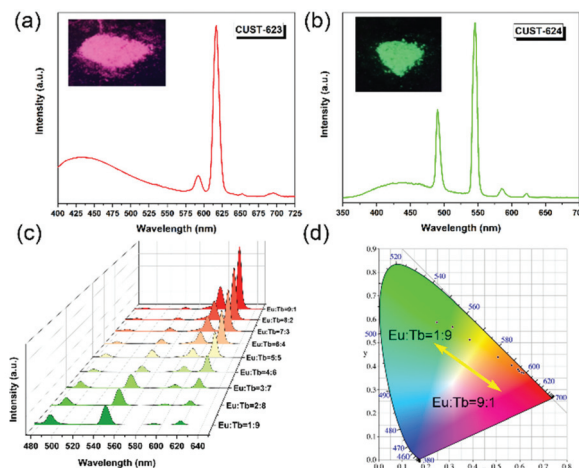

Fig. 2 Fluorescence spectra of solid CUST-623 (a), CUST-624 (b) and $Eu_xTb_{0.02-x}$-MOFs (c). (d) CIE of $Eu_xTb_{0.02-x}$-MOFs. Inset: a picture of CUST-623 and CUST-623 under a UV-lamp.

3.4. Characterization of Ln-MOFs@PVA

$Eu_xTb_{0.02-x}$-BDPO crystal powders were immersed in water through sonication to make a suspension. The suspension is thoroughly mixed with an aqueous solution of PVA by stirring, and subsequently poured into the mold to prepare the films. $Eu_xTb_{0.02-x}$-BDPO@PVA films show the integrated structure and performance of MOFs and polymers. The PXRD patterns of $Eu_xTb_{0.02-x}$-BDPO@PVA reveal the characteristic peaks of the Ln-MOFs, confirming that Ln-MOF particles retain good crystallinity during the preparation process (Fig. S7†). The FT-IR spectra also prove the presence of Ln-MOFs (Fig. S8†). The scanning electron microscopy (SEM) images of the $Eu_{0.002}Tb_{0.018}$-BDPO@PVA membrane show the surface and cross-sections, in which MOF particles are uniformly dispersed in the membrane. Meanwhile, EDS mapping images further confirm the uniform dispersion of intact MOF particles (Fig. 3e and f). $Eu_{0.002}Tb_{0.018}$-BDPO@PVA can be bent at will, manifesting excellent processing performance (Fig. 3g). Meanwhile, CUST-623@PVA and CUST-624@PVA display the fluorescence properties from pristine MOFs (Fig. S9†).

3.5. Temperature sensing

The temperature dependence of CUST-623, CUST-624 and $Eu_xTb_{0.02-x}$-BDPO doping systems was studied systematically. From 303 K to 423 K, the fluorescence intensity of CUST-623 and CUST-624 gradually weakens as the temperature increases (Fig. 4a and b). To evaluate the ratiometric luminescent thermometer potential for the Eu and Tb mixed system, $Eu_{0.002}Tb_{0.018}$-BDPO as a representative was investigated systematically. With the increase of temperature from 303 K to 423 K, the fluorescence intensity of Eu^{3+} ions ($^5D_0$–$^7F_2$) slowly decreases, while the fluorescence intensity of Tb^{3+} ions ($^5D_4$–$^7F_5$) drops significantly (Fig. 4c and d), which can be explained by the energy transfer from Tb to Eu. The emission intensity ratio of the Tb^{3+} ($^5D_4 \rightarrow {}^7F_5$, 545 nm) to Eu^{3+} ($^5D_0 \rightarrow$
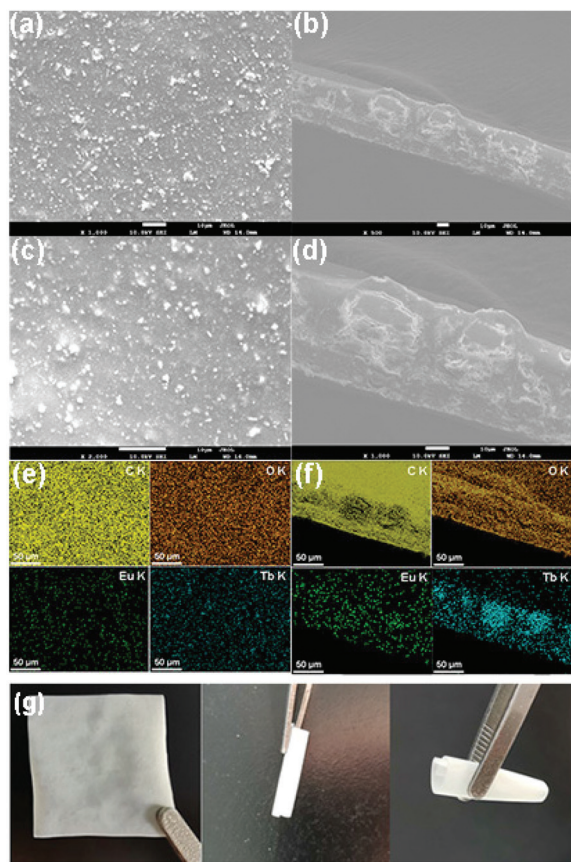
Fig. 3 (a) and (c) Plane SEM images of $Eu_{0.002}Tb_{0.018}$-BDPO@PVA. (b) and (d) Cross section SEM images of $Eu_{0.002}Tb_{0.018}$-BDPO@PVA. (e) (f) The corresponding EDS mapping. (g) Processability of $Eu_{0.002}Tb_{0.018}$-BDPO@PVA.
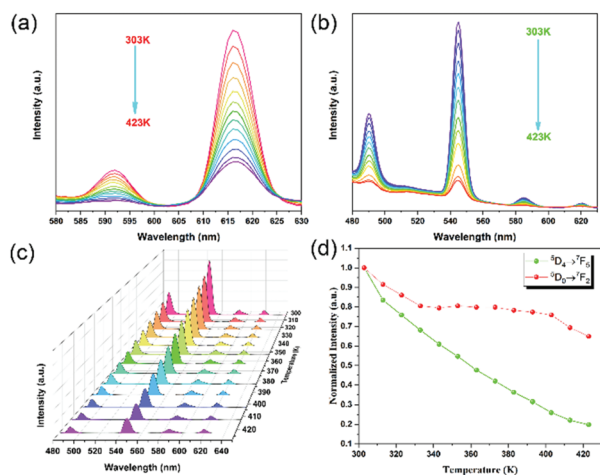

Fig. 4 Emission spectra of CUST-623 (a), CUST-624 (b) and $Eu_{0.002}Tb_{0.018}$-BDPO (c) recorded at 303 K–423 K. (d) The normalized intensities of $Eu_{0.002}Tb_{0.018}$-BDPO.

$^7F_2$, 617 nm) transition (I_{Tb}/I_{Eu}) demonstrates a good linear relationship with increasing temperature (Fig. S10a†), so the $Eu_{0.002}Tb_{0.018}$-BDPO can be used as a ratiometric luminescent

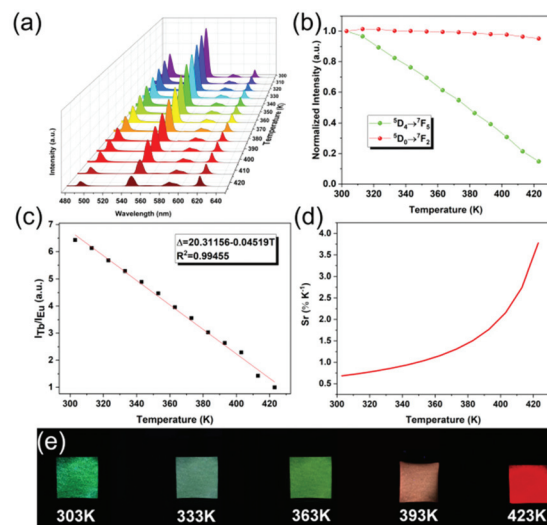**Fig. 5** (a) Emission spectra of $Eu_{0.002}Tb_{0.018}$-BDPO@PVA recorded at 303 K–423 K. (b) The normalized intensities of $Eu_{0.002}Tb_{0.018}$-BDPO@PVA. (c) Fitted curves of the integrated intensity ratio for $Eu_{0.002}Tb_{0.018}$-BDPO@PVA. (d) Relative sensitivity of $Eu_{0.002}Tb_{0.018}$-BDPO@PVA. (e) The luminescence picture of $Eu_{0.002}Tb_{0.018}$-BDPO@PVA under the UV lamp from 303 K to 423 K.

thermometer. The sensitivity is 2.4% K^{-1} at 423 K (Fig. S10b†). $Eu_{0.004}Tb_{0.016}$-BDPO also displays a similar phenomenon, with a maximum sensitivity of 1.7% K^{-1} at 423 K (Fig. S11†). The above result illustrates that $Eu_xTb_{0.02-x}$-BDPO can be promising as excellent sensors in non-contact temperature measurements. Meanwhile, the energy transfer process is necessary to construct a proportional luminescent thermometer. The energy level diagram also confirms the energy difference between Tb^{3+} and Eu^{3+}.[25] As the temperature increases, energy shifts from Tb^{3+} to Eu^{3+} (Scheme 1). Compared with ratiometric luminescent thermometers, $Eu_{0.002}Tb_{0.018}$-BDPO and $Eu_{0.004}Tb_{0.016}$-BDPO as ratiometric luminescent thermometers possess great merits in the sensitivity and applicable temperature range (Table S5†).

$Eu_{0.002}Tb_{0.018}$-BDPO@PVA also exhibits excellent temperature dependence (Fig. 5a and b). At 303–423 K, the emission intensity ratio (I_{Tb}/I_{Eu}) of Tb^{3+} to Eu^{3+} features a good linear relationship with temperature (Fig. 5c) and the relationship can be expressed as: $\Delta = 20.31156 - 0.04519\,T$. The maximum sensitivity of $Eu_{0.002}Tb_{0.018}$-BDPO@PVA is 3.7% K^{-1} at 423 K (Fig. 5d). The result indicates that the $Eu_{0.002}Tb_{0.018}$-BDPO@PVA membrane can be used as a good candidate for membrane self-referencing ratiometric luminescent thermometers. Under the ultraviolet lamp, the color of the membrane changes from green to red as the temperature increases, which can be observed with the naked eye (Fig. 5e).

3.6. Chemical sensing

Iron and chromium ions play significant roles in industrial production, and iron ions are also essential trace elements for the human body. However, excessive intake of heavy metals in
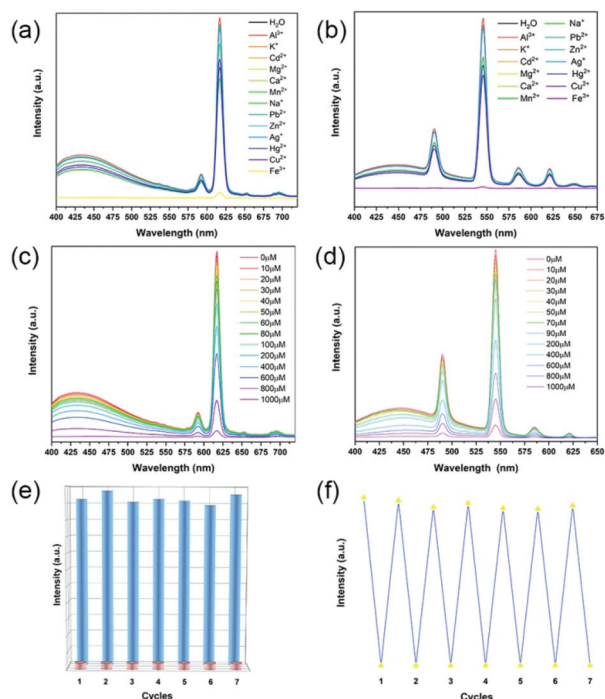
3262 | *Inorg. Chem. Front.*, 2022, **9**, 3259–3266

This journal is © the Partner Organisations 2022

Fig. 6 Fluorescence spectra of CUST-623 (a) and CUST-624 (b) in metal ion aqueous solution. Fluorescence spectra of CUST-623 (c) and CUST-624 (d) upon incremental addition of Fe^{3+}. Titration and cycling tests of CUST-623 (e) and CUST-624 (f) in water of Fe^{3+} ions.
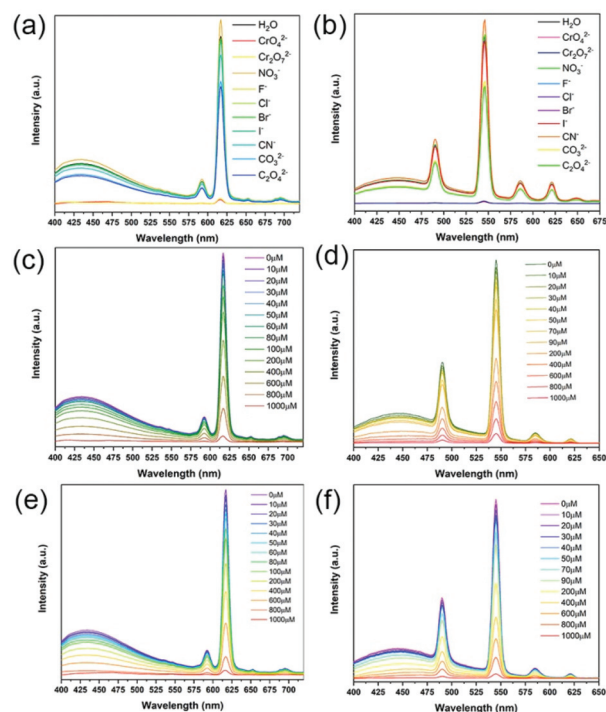

Fig. 7 Fluorescence spectra of CUST-623 (a) and CUST-624 (b) in anion aqueous solution. Fluorescence spectra of CUST-623 (c) and CUST-624 (d) upon incremental addition of $Cr_2O_7^{2-}$. Fluorescence spectra of CUST-623 (e) and CUST-624 (f) upon incremental addition of CrO_4^{2-}.

the human body can cause a range of health problems, including organ failure, neurological diseases, cancer, *etc.* Owing to their excellent stability in water and unique light-emitting characteristics, CUST-623 and CUST-624 can be used as promising fluorescent sensors for detecting noxious substances in water. CUST-623 and CUST-624 were soaked in solutions containing different metal ions to observe fluorescence intensity changes. When Fe^{3+} ions were added, the fluorescence intensity of CUST-623 and CUST-624 arose quenching (Fig. 6a and b). To further explore the quenching effect of Fe^{3+} ions, fluorescence titration experiments were carried out in a continuous concentration range. As the concentration of Fe^{3+} ions increases, the fluorescence intensity decreases (Fig. 6c and d), and the quenching efficiency is linear in a low concentration range (0–100 μM) (Fig. S12†). After being mixed with other metal ions, Fe^{3+} ions can still exhibit an excellent quenching effect on CUST-623 and CUST-624 (Fig. S13†). After seven cycles of experiments, the results prove fabulous recyclability of CUST-623 and CUST-624 (Fig. 6e and f). In a likely manner, the fluorescence intensity of CUST-623 and CUST-624 is also rapidly decreased by $Cr_2O_7^{2-}$ and CrO_4^{2-} (Fig. 7). Circulatory experiments demonstrate that CUST-623 and CUST-624 manifest ideal cycling performance (Fig. S14†). The quenching efficiency is linear in the concentration range of 0–100 μM (Fig. S15†). Meantime, CUST-623 and CUST-624 express excellent anti-interference when detecting $Cr_2O_7^{2-}$ and CrO_4^{2-} (Fig. S16†). The R^2, K_{sv} constants and DOLs of

Table 1 R^2, K_{sv} constant, and the detection limit for the detection of Fe^{3+}, $Cr_2O_7^{2-}$, CrO_4^{2-} and TNP by CUST-623 and CUST-624

	CUST-623			CUST-624		
	R^2	K_{sv}	DOLs	R^2	K_{sv}	DOLs
Fe^{3+}	0.9875	2.44×10^4	1.17 μM	0.9935	2.07×10^4	1.31 μM
$Cr_2O_7^{2-}$	0.9930	3.26×10^4	0.88 μM	0.9855	4.01×10^4	0.68 μM
CrO_4^{2-}	0.9883	3.54×10^4	0.81 μM	0.9882	3.25×10^4	0.83 μM
TNP	0.9878	6.03×10^5	0.21 μM	0.9941	6.288×10^5	0.20 μM

CUST-623 and CUST-624 detection ions are summarized in Table 1.

As a class of nitroaromatic molecules, nitro explosives are highly toxic and extremely explosive, requiring fast and susceptible detection in water. Hence, the sensing experiments of nitro explosives by CUST-623 and CUST-624 were studied systematically. We selected several ordinary nitroaromatic explosives, including 1,3-dinitrobenzene (1,3-DNB), 1,2-dinitrobenzene (1,2-DNB), nitrobenzene (NB), 1,4-dinitrobenzene (1,4-DNB) and 2,4,6-trinitrophenol (TNP). The luminescence intensity of CUST-623 and CUST-624 is distinctly lessened in TNP solution (Fig. 8). The *S*–*V* plots of CUST-623 and CUST-624 are nearly linear in low concentrations (Fig. S17†). Meanwhile, CUST-623 and CUST-624 display excellent anti-interference (Fig. S18†) and cycling performance (Fig. 8e and f). The values of R^2, K_{sv} constants, and DOLs for the detection of TNP by

This journal is © the Partner Organisations 2022

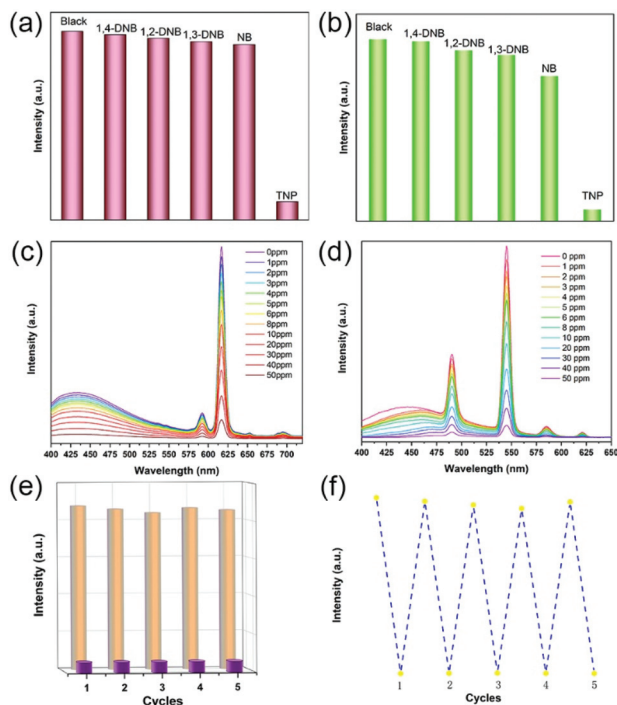*Inorg. Chem. Front.*, 2022, **9**, 3259–3266 | **3263**

Fig. 8 Fluorescence intensity of CUST-623 (a) and CUST-624 (b) in aqueous solutions of nitro explosives. Fluorescence spectra of CUST-623 (c) and CUST-624 (d) upon incremental addition of TNP. Titration and cycling tests of CUST-623 (e) and CUST-624 (f) in the solution of TNP.

CUST-623 and CUST-624 are shown in Table 1. For accomplishing ratiometric fluorescence sensing and visual detection,[26,27] we investigated the sensing effect of the doping system for several harmful substances. A quenching response is shown. The quenching efficiency of the detected substances for Eu^{3+} and Tb^{3+} is almost the same, similar to the quenching efficiency for single CUST-623 and CUST-624. Therefore, the effect of visual inspection is not obvious (Fig. S19†).

3.7. Luminescence quenching mechanism

To investigate the mechanism of fluorescence quenching, IR, PXRD and UV tests were carried out on the crystals soaked in solutions containing ions or TNP. First, the infrared spectra of CUST-623 and CUST-624 did not change before and after immersion, indicating that the test substance did not react with the crystal (Fig. S20†).[28] In addition, the peaks in the PXRD patterns of the immersed crystal powders are consistent with the fitted peaks, indicating the intact crystal structure without framework collapse (Fig. S21 and S22†).[29] Finally, in the UV absorption spectra, CUST-623 and CUST-624 exhibit a large degree of overlap with Fe^{3+}, $Cr_2O_7^{2-}$, CrO_4^{2-}, and TNP (Fig. S23†).[30] Therefore, the reason for the quenching of the fluorescence sensing can be explained by resonance energy transfer. The fluorescence excitation spectra of CUST-623 and CUST-624 overlap with the ultraviolet visible absorption

spectra of the detected substances (Fig. S24†), showing that the fluorescence quenching is also due to the fluorescence resonance energy transfer process.[31]

4.   Conclusions

In summary, five lanthanide MOFs based on ligands were successfully prepared. Among them, CUST-623 and CUST-624 exhibit excellent fluorescence characteristics, used for temperature and chemical sensing. $Eu_{0.002}Tb_{0.018}$-MOF possesses potential as a ratiometric luminescent thermometer. At the same time, the combination of MOFs with the polymer can further enhance the fluorescence properties. CUST-623 and CUST-624 manifest high stability and recyclability as fluorescent sensors for detecting $Cr_2O_7^{2-}$, CrO_4^{2-}, Fe^{3+} and TNP. On the whole, Ln-MOFs are expected to be applied as ideal chemical sensors and ratiometric luminescent thermometers.

Author contributions

The authors contributed equally to this work.

Conflicts of interest

There are no conflicts to declare.

Acknowledgements

Notes and references

1 (a) H. He, Q. Sun, W. Gao, J. A. Perman, F. Sun, G. Zhu, B. Aguila, K. Forrest, B. Space and S. Ma, A stable metal-organic framework featuring a local buffer environment for carbon dioxide fixation, *Angew. Chem., Int. Ed.*, 2018, **57**, 4657–4662; (b) W. P. Lustig, S. Mukherjee, N. D. Rudd, A. V. Desai, J. Li and S. K. Ghosh, Metal–organic frameworks: functional luminescent and photonic materials for sensing applications, *Chem. Soc. Rev.*, 2017, **46**, 3242–3285.

2 (a) M. K. Goshisht and N. Tripathi, Fluorescence-based sensors as an emerging tool for anion detection: mechanism, sensory materials and applications, *J. Mater. Chem. C*, 2021, **9**, 9820–9850; (b) H. Wang, P. W. Lusting and J. Li, Sensing and capture of toxic and hazardous gases and

3264 | *Inorg. Chem. Front.*, 2022, **9**, 3259–3266

This journal is © the Partner Organisations 2022

vapors by metal-organic frameworks, *Chem. Soc. Rev.*, 2018, **47**, 4729–4756.

3 (*a*) P. L. Wang, L. H. Xie, E. A. Joseph, J. R. Li, X. O. Su and H. C. Zhou, Metal–organic frameworks for food safety, *Chem. Rev.*, 2019, **119**, 10638–10690; (*b*) Y. Xu, Y. Y. Zhou, M. Yu, Y. Xiong, X. G. Liu and Z. Zhao, Excellent quantum yield enhancement in luminescent metal-organic layer for sensitive detection of antibiotics in aqueous medium, *Dyes Pigm.*, 2022, **198**, 109961.

4 (*a*) C. M. Wu, Z. Feng, H. Q. Zhou, F. Yu, J. R. Li, X. H. Ye and J. He, Metal-organic frameworks constructed from tri-valent lanthanide nodes (Eu3$^+$, Tb3$^+$, and Dy^{3+}) and thio-phenethio-functionalized linker with photoluminescent response selective towards Ag$^+$ ions, *Dyes Pigm.*, 2022, **198**, 109999; (*b*) B. Qin, X. Zhang, J. Qiu, G. Gahungu, H. Yuan and J. Zhang, Water-Robust Zinc-Organic Framework with Mixed Nodes and Its Handy Mixed-Matrix Membrane for Highly Effective Luminescent Detection of Fe^{3+}, CrO42−, and Cr2O72− in Aqueous Solution, *Inorg. Chem.*, 2021, **60**, 1716–1725; (*c*) J. Zhang, S. Ren, H. Xia, W. Jia and C. Zhang, AIE-ligand-based luminescent Cd (ii)–organic framework as the first "turn-on" Fe3+ sensor in aqueous medium, *J. Mater. Chem. C*, 2020, **8**, 1427–1432.

5 (*a*) X. Wang, M. Lei, T. Zhang, Q. Zhang, R. Zhang and M. Yang, A water-stable multi-responsive luminescent Zn-MOF sensor for detecting TNP, NZF and Cr2O72- in aqueous media, *Dalton Trans.*, 2021, **50**, 3816–3824; (*b*) K. Vaid, J. Dhiman, S. Kumar, K. H. Kim and V. Kumar, Mixed metal (cobalt/molybdenum) based metal-organic frameworks for highly sensitive and specific sensing of arsenic(v): Spectroscopic versus paper-based approaches, *Chem. Eng. J.*, 2021, **426**, 131243; (*c*) M. Chhatwal, R. Mittal, R. D. Gupta and S. K. Awasthi, Sensing ensembles for nitroaromatics, *J. Mater. Chem. C*, 2018, **6**, 12142–12158; (*d*) P. Rani, Gauri, A. Husain, K. K. Bhasin and G. Kumar, A Doubly Interpenetrated CuII Metal–Organic Framework for Selective Molecular Recognition of Nitroaromatics, *Cryst. Growth Des.*, 2020, **20**, 7141–7151.

6 (*a*) J. J. Zhao, P. Y. Liu, L. J. Song, L. Zhang, Z. L. Liu and Y. Q. Wang, A water stable Eu(iii)-organic framework as a recyclable multi-responsive luminescent sensor for efficient detection of p-aminophenol in simulated urine, and Mn-VII and Cr-VI anions in aqueous solutions, *Dalton Trans.*, 2021, **50**, 5236–5243; (*b*) H. Yang, J. Liu, L. Wang, L. Ma, F. Nie and G. Yang, Metal-organic framework as a mimetic enzyme with excellent adaptability for sensitive chemilumi-nescence detection of glutathione in cell lysate, *Talanta*, 2022, **238**, 123041; (*c*) A. Li, Q. Chu, H. Zhou, Z. Yang, B. Liu and J. Zhang, Effective nitenpyram detection in a dual-walled nitrogen-rich In (iii)/Tb (iii)–organic frame-work, *Inorg. Chem. Front.*, 2021, **8**, 2341–2348.

7 (*a*) S. Wu, M. Zhu, Y. Zhang, M. Kosinova, V. P. Fedin and E. Gao, A Water–Stable Lanthanide Coordination Polymer as Multicenter Platform for Ratiometric Luminescent Sensing Antibiotics, *Chem. – Eur. J.*, 2020, **26**, 3137–3144; (*b*) Y. Cui, F. Zhu, B. Chen and G. Qian, Metal–organic

frameworks for luminescence thermometry, *Chem. Commun.*, 2015, **51**, 7420–7431.

8 X. Lin, M. Kong, N. Wu, Y. Gu, X. Qiu, X. Chen and F. Li, Measurement of Temperature Distribution at the Nanoscale with Luminescent Probes Based on Lanthanide Nanoparticles and Quantum Dots, *ACS Appl. Mater. Interfaces*, 2020, **12**, 52393–52401.

9 (*a*) X. Rao, T. Song, J. Gao, Y. Cui, Y. Yang, C. Wu, B. Chen and G. Qian, A Highly Sensitive Mixed Lanthanide Metal-Organic Framework Self-Calibrated Luminescent Thermometer, *J. Am. Chem. Soc.*, 2013, **135**, 15559–15564; (*b*) Y. Yang, Y. Wang, Y. Feng, X. Song, C. Cao, G. Zhang and W. Liu, Three isostructural Eu3+/Tb3+ co-doped MOFs for wide-range ratiometric temperature sensing, *Talanta*, 2020, **208**, 120354.

10 D. A. Gálico and M. Murugesu, Inside-Out/Outside-In Tunability in Nanosized Lanthanide-Based Molecular Cluster-Aggregates: Modulating the Luminescence Thermometry Performance via Composition Control, *ACS Appl. Mater. Interfaces*, 2021, **13**, 47052–47060.

11 V. Trannoy, A. N. Carneiro Neto, C. D. Brites, L. D. Carlos and H. Serier-Brault, Engineering of Mixed Eu3+/Tb3+ Metal-Organic Frameworks Luminescent Thermometers with Tunable Sensitivity, *Adv. Opt. Mater.*, 2021, **9**, 2001938.

12 Y. Chen, J. Qiu, Z. Chen, Y. Zhao, B. Li and C. Zeng, New luminescent lanthanide complexes and Tb, Eu co-doped complex as a wide temperature self-calibrating thermo-meter, *Dyes Pigm.*, 2021, **194**, 109671.

13 H. J. Chen, L. Q. Chen, L. R. Lin, L. S. Long and L. S. Zheng, Doped Luminescent Lanthanide Coordination Polymers Exhibiting both White-Light Emission and Thermal Sensitivity, *Inorg. Chem.*, 2021, **60**, 6986–6990.

14 (*a*) É. Whelan, F. W. Steuber, T. Gunnlaugsson and W. Schmitt, Tuning photoactive metal–organic frameworks for luminescence and photocatalytic applications, *Chem. Soc. Rev.*, 2021, **437**, 213757; (*b*) Y. Zhang, S. Liu, Z. S. Zhao, Z. Wang, R. Zhang, L. Liu and Z. B. Han, Recent progress in lanthanide metal–organic frameworks and their deriva-tives in catalytic applications, *Inorg. Chem. Front.*, 2021, **8**, 590–619; (*c*) C. Niu, L. Qian, Y. Pei, P. Qi, X. Hu, R. Li and Y. Xing, Preparation and photoluminescence of functiona-lized cotton fabric by double luminescent guests-encapsu-lated ZnBDC metal-organic framework, *Dyes Pigm.*, 2022, **197**, 109835; (*d*) J. Wang, D. Li, Y. Ye, Y. Qiu, J. Liu, L. Huang, B. Liang and B. Chen, A Fluorescent Metal-Organic Framework for Food Real-Time Visual Monitoring, *Adv. Mater.*, 2021, **33**, 2008020.

15 (*a*) L. Chen, D. H. Liu, J. Peng, Q. Z. Du and H. He, Ratiometric luminescence sensing of metal-organic frame-works: Tactics and perspectives, *Coord. Chem. Rev.*, 2020, **404**, 213113; (*b*) H. Chen, Z. Zhang, T. Hu and X. Zhang, An NH2-modified {Eu III2}–organic framework for the efficient chemical fixation of CO2 and highly selective sensing of 2, 4, 6-trinitrophenol, *Inorg. Chem. Front.*, 2021, **8**, 4376–4385; (*c*) S. Wang, B. Sun, J. Sun, X. Hao, X. Li, C. Zhou and Z. Su, Lanthanide metal−organic frameworks based on

This journal is © the Partner Organisations 2022

Inorg. Chem. Front., 2022, **9**, 3259–3266 | **3265**

planar π-conjugated ligands for white light emission, temperature and chemical sensing, *Dyes Pigm.*, 2022, **202**, 110256.

16 X. Meng, S. Y. Song, X. Z. Song, M. Zhu, S. N. Zhao, L. L. Wu and H. J. Zhang, A Eu/Tb-codoped coordination polymer luminescent thermometer, *Inorg. Chem. Front.*, 2014, **1**, 757–760.

17 (*a*) H. Q. Yin and X. B. Yin, Metal-Organic Frameworks with Multiple Luminescence Emissions: Designs and Applications, *Acc. Chem. Res.*, 2020, **53**, 485–495; (*b*) Y. Cui, D. Yue, Y. Huang, J. Zhang, Z. Wang, D. Yang and G. Qian, Photo-induced electron transfer in metal-organic framework: a new approach towards highly sensitive luminescent probe of Fe3+, *Chem. Commun.*, 2019, **55**, 11231–11234; (*c*) M. Y. Fan, H. H. Yu, P. Fu, Z. M. Su, X. Li, X. L. Hu, F. W. Gao and Q. Q. Pan, Luminescent Cd(ɪɪ) metal-organic frameworks with anthracene nitrogen-containing organic ligands as novel multifunctional chemosensors for the detection of picric acid, pesticides, and ferric ions, *Dyes Pigm.*, 2021, **185**, 108834.

18 (*a*) Y. Yang, L. Li, H. Yang and L. Sun, Five Lanthanide-Based Metal–Organic Frameworks Built from a π-Conjugated Ligand with Isophthalate Units Featuring Sensitive Fluorescent Sensing for DMF and Acetone Molecules, *Cryst. Growth Des.*, 2021, **21**, 2954–2961; (*b*) J. C. Santos, Y. Pramudya, M. Krstić, D. H. Chen, B. L. Neumeier, C. Feldmann and E. Redel, Halogenated Terephthalic Acid "Antenna Effects" in Lanthanide-SURMOF Thin Films, *ACS Appl. Mater. Interfaces*, 2020, **12**, 52166–52174.

19 (*a*) Y. Jiang, Y. Huang, X. Shi, Z. Lu, J. Ren, Z. Wang and L. Wang, Eu-MOF and its mixed-matrix membranes as a fluorescent sensor for quantitative ratiometric pH and folic acid detection, and visible fingerprint identifying, *Inorg. Chem. Front.*, 2021, **8**, 4924–4932; (*b*) J. Dechnik, J. Gascon, C. J. Doonan, C. Janiak and C. J. Sumby, Mixed–matrix membranes, *Angew. Chem., Int. Ed.*, 2017, **56**, 9292–9310.

20 Y. Ding, Y. Lu, K. Yu, S. Wang, D. Zhao and B. Chen, MOF-Nanocomposite Mixed-Matrix Membrane for Dual-Luminescence Ratiometric Temperature Sensing, *Adv. Opt. Mater.*, 2021, **9**, 2100945.

21 J. Troyano, O. Castillo, J. I. Martínez, V. Fernández-Moreira, Y. Ballesteros, D. Maspoch and S. Delgado, Reversible Thermochromic Polymeric Thin Films Made of Ultrathin 2D Crystals of Coordination Polymers Based on Copper(ɪ)-Thiophenolates, *Adv. Funct. Mater.*, 2018, **28**, 1704040.

22 T. Feng, Y. Ye, X. Liu, H. Cui, Z. Li, Y. Zhang, B. Liang, H. Li and B. Chen, A Robust Mixed-Lanthanide PolyMOF Membrane for Ratiometric Temperature Sensing, *Angew. Chem., Int. Ed.*, 2020, **59**, 21752–21757.

23 H. Q. Yin, X. Y. Wang and X. B. Yin, Rotation restricted emission and antenna effect in single metal–organic frameworks, *J. Am. Chem. Soc.*, 2019, **141**, 15166–15173.

24 X. Y. Li, W. J. Shi, X. Q. Wang, L. N. Ma, L. Hou and Y. Y. Wang, Luminescence modulation, white light emission, and energy transfer in a family of lanthanide metal–organic frameworks based on a planar π-conjugated ligand, *Cryst. Growth Des.*, 2017, **17**, 4217–4224.

25 F. Chen, Y. M. Wang, W. Guo and X. B. Yin, Color-tunable lanthanide metal–organic framework gels, *Chem. Sci.*, 2019, **10**, 1644–1650.

26 Y. Cui, F. Chen and X. B. Yin, A ratiometric fluorescence platform based on boric-acid-functional Eu-MOF for sensitive detection of H_2O_2 and glucose, *Biosens. Bioelectron.*, 2019, **135**, 208–215.

27 Y. M. Wang, Z. R. Yang, L. Xiao and X. B. Yin, Lab-on-MOFs: Color-Coded Multitarget Fluorescence Detection with White-Light Emitting Metal–Organic Frameworks under Single Wavelength Excitation, *Anal. Chem.*, 2018, **90**, 5758–5763.

28 M. Y. Fan, B. Sun, X. Li, Q. Q. Pan, J. Sun, P. Ma and Z. M. Su, Highly Fluorescent Cadmium Based Metal–Organic Frameworks for Rapid Detection of Antibiotic Residues, Fe3+ and Cr2O72− Ions, *Inorg. Chem.*, 2021, **60**, 9148–9156.

29 D. Wang, Z. Y. Hu, S. S. Xu, D. D. Li, Q. Zhang, W. Ma, H. P. Zhou, J. Y. Wu and Y. P. Tian, Fluorescent metal-organic frameworks based on mixed organic ligands: new candidates for highly sensitive detection of TNP, *Dalton Trans.*, 2019, **48**, 1900.

30 J. Zhang, J. Wu, G. Tang, J. Feng, F. Luo, B. Xu and C. Zhang, Multiresponsive water-stable luminescent Cd coordination polymer for detection of TNP and Cu2+, *Sens. Actuators, B*, 2018, **272**, 166–174.

31 L. L. Qian, Z. X. Wang, J. G. Ding, H. X. Tian, K. Li, B. L. Li and H. Y. Li, A 2D copper(ɪ) metal-organic framework: synthesis, structure and luminescence sensing for cupric, ferric, chromate and TNP, *Dyes Pigm.*, 2020, **175**, 108159.

3266 | *Inorg. Chem. Front.*, 2022, **9**, 3259–3266

This journal is © the Partner Organisations 2022